Int. J. Electrochem. Sci., 8 **(2013)** 12801 - 12815

International Journal of
ELECTROCHEMICAL
SCIENCE
www.electrochemsci.org

Cold Rolling Effect on the Microstructure and Pitting Resistance of the NBR ISO 5832-1 Austenitic Stainless Steel

Alexander Hincapie Ramirez, Cristiaann Hincapie Ramirez, Isolda Costa[*]

Instituto de Pesquisas Energéticas e Nucleares, IPEN/CNEN-SP, Centro de Ciência e Tecnologia de Materiais (CCTM), Av. Prof. Lineu Prestes, 2242, CEP 05508-000, São Paulo-SP/Brazil.
[*]E-mail: icosta@ipen.br

Received: 14 July 2013 / *Accepted:* 6 September 2013 / *Published:* 20 October 2013

The aim of this work is to assess the influence of cold rolling on the microstructure and pitting resistance of the NBR ISO 5832-1 austenitic stainless steel. Samples of this stainless steel either with deformation, corresponding to 30%, 50% and 70% of reduction in thickness induced by cold rolling, or without deformation (as received), were characterized regarding their microstructure to investigate the metallurgical effects created during the deformation process. The results showed that certain levels of cold rolling (30% and 50%) decreased the corrosion resistance of the stainless steel by causing inclusions fragmentation and voids at the matrix-inclusion interface, whereas unexpectedly, high levels of cold deformation (70%) resulted in improved localized corrosion resistance. Surface observation showed that for this level of deformation, the voids created by fragmentation and the matrix-inclusion interface were shielded with matrix material.

Keywords: Corrosion, Cold Deformation, Microstructural effects, NBR ISO 5832-1 austenitic stainless steel, Biomaterials.

1. INTRODUCTION

Stainless steels (SS) are widely used in different types of industries due to their mechanical and corrosion properties[1]. Depending on their final applications, many alloying elements, besides nickel and chromium, are added into the SS to increase their mechanical and corrosion properties. The corrosion resistance of stainless steels is strongly affected by their chemical composition[2,3]. Among the stainless steels, the austenitic types are considered one of the most corrosion resistant stainless steels when exposed to industrial atmospheres or acidic aggressive media [4]. The chromium content in the stainless steel is one of the most important factors for its corrosion resistance. Furthermore, the

molybdenum content is another important aspect that contributes to the pitting corrosion resistance of the austenitic stainless steels in chloride containing media [5].

The influence of cold deformation on the pitting corrosion resistance, including its initiation, propagation and repassivation has also been reported [6-8]. Most studies [7,8] indicated that cold deformation produces a harmful effect on the corrosion resistance of the material. The effect of the cold deformation on the higher susceptibility to pitting corrosion resistance of the material has been explained by different mechanisms [7,9,10]. The first associated it to the additional energy introduced to the material by deformation, decreasing the resistance of the material to localized corrosion [7]. A second related the increase in pitting susceptibility to the effect of cold working on the to deformed material microstructure and its grain orientation (texture) [9,10]. During the cold deformation, the inclusions often act as preferential sites for defects, once non-metallic inclusions can be fragmented, or microcracks might be formed at the matrix/inclusion interface [11]. However, preliminary investigations carried out in our laboratory showed that there is not a clear relation between cold deformation and corrosion resistance. The aim of this work is to assess the influence of cold rolling of the NBR ISO 5832-1 austenitic stainless steel on its microstructure and passive film properties.

2. MATERIALS AND METHODS

The material used in this investigation consisted of the ISO NBR 5832-1 stainless steel (SS) whose chemical composition is shown in Table 1. This SS is largely used for biomedical applications, mainly for the fabrication of metallic implants.

Table 1. Chemical composition (wt. %) of ISO NBR 5832-1 stainless steel tested.

Cr	Ni	Mo	Mn	S	Si	C	P	Fe
18.32	14.33	2.59	2.09	0.0003	0.378	0.023	0.026	Bal

Prior to immersion tests, the surface for exposure to the electrolyte was prepared by wet ground with silicon carbide paper up to 1200 mesh. Subsequently, the surface was polished with diamond suspension up to a finishing of 1 micron. Finally, the samples were degreased with ethanol, rinsed with deionized water and dried under hot air stream. The electrochemical tests were carried out in a flat cell with an Ag/AgCl reference electrode and a platinum wire counter electrode. The electrolyte used in this study was based on a phosphate buffer solution that simulates the composition of body fluids but the salts composition was increased 6.5 times to increase its corrosivity. The chemical composition of the electrolyte used was: 58.41 g/L NaCl, 9.21 g/L Na_2HPO_4, 17.7 g/L KH_2PO_4.

In order to investigate the resistance to passive film breakdown, samples were anodically polarized. Potentiodynamic polarization tests were performed at a scan rate of 1mV s^{-1}. Polarization

was carried from -20 mV relatively to the open circuit potential (OCP) into the anodic direction. When the current density reached nearly 10^{-3} A cm^{-2} the direction of polarization was reversed and the polarization ended when the final potential achieved approximately -150 mV vs $E_{Ag/AgCl}$. In order to investigate reproducibility of the results, each condition investigated was tested at least three times, allowing to obtain both the mean value and standard deviation of the breakdown potential (E_{break}).

Some anodic polarization tests were also carried out in order to investigate the correlation between the microstructure and passive film breakdown. For this purpose, polarization was interrupted when the current density started increasing and reached nearly 10^{-4} A cm^{-2}. The polarized surface of the samples was examined by means of Scanning Electron Microscopy (SEM) in search of the nucleation sites and their relation to the stainless steel microstructure.

Electrochemical impedance spectroscopy measurements were performed at the open circuit potential in the frequency range from 100 kHz to 10 mHz, using a sinusoidal signal with amplitude of 10 mV.

3. RESULTS AND DISCUSSION

3.1. Microstructure characterization

The microstructure of the ISO NBR 5832-1 austenitic stainless as received is shown in Figure 1. The grains of austenite phase and a few twins are seen in this microstructure, but no precipitates are evidenced at the magnification of this figure.

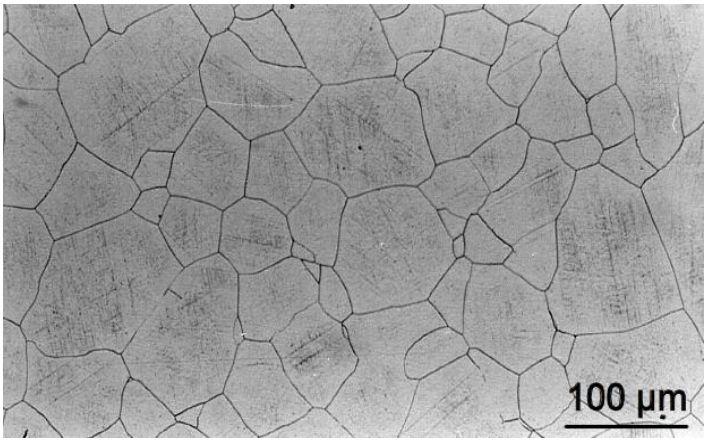

Figure 1. Microstructure of the ISO NBR 5832-1 used in this study.

Figure 1 clearly shows an austenitic structure with very few twins, indicating that the material has not been deformed and also there is no evidence of precipitates, due to the low concentration of interstitials in the alloy. The precipitates present in this material are too small to be revealed by optical microscopy. Techniques of higher magnifications, such as electronic microscopy, are necessary to investigate the presence of inclusion.

In order to evaluate the correlation between the nucleation of pits and microstructural characteristics, a few polarization tests were carried out where the polarization test was interrrupted once the current density started to increase, at very low current densities (10^{-5} A.cm^{-2}) and the surface of the polarized samples was observed by scanning electron microscopy and analysed by energy dispersive spectrometry (EDS). Surface observation showed that the early pits were always connected to non-metallic inclusions. Consequently, to determine the role of inclusions on pitting corrosion resistance, characterization of inclusions was performed for the SS in the various conditions tested, prior an after the corrosion tests.

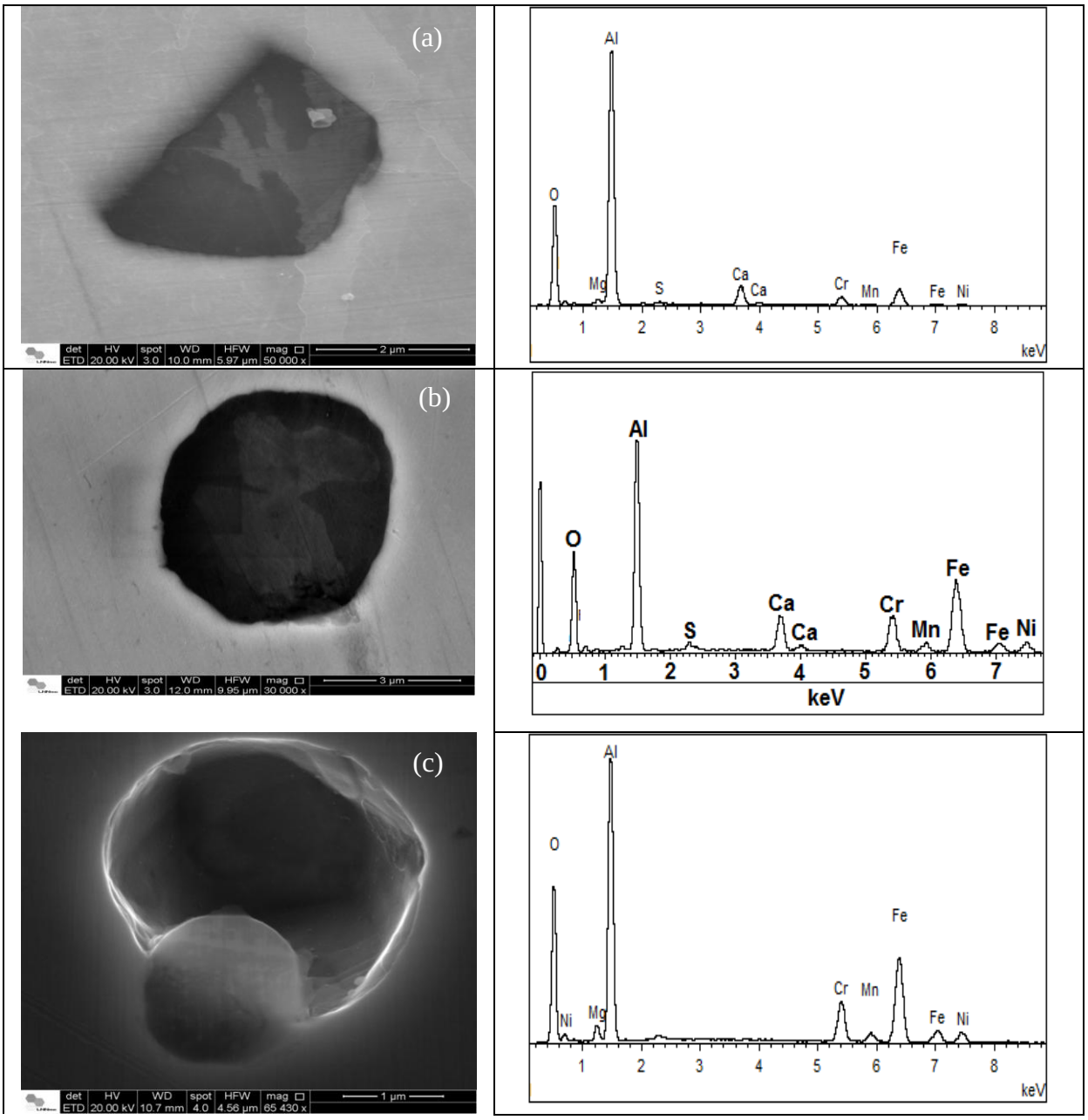

Figure 2. Types of inclusions found in the NBR 5832-1 stainless steel in the as received condition. (a) and (a) complex inclusion composed by a mixture of alumina containing calcium and sulphur, and (c) pure alumina inclusion.

The surface characterization of the tested samples showed that the ISO NBR 5832-1 austenitic stainless steel presented various types of inclusions in its microstructure, such as: mixed inclusions of aluminium oxide containing calcium and sulphur (Figure 2 (a) and (b)), and a pure alumina inclusion (Figure 2 (c)). It is important to note that no defects are associated to such inclusions, neither fragmentation nor the formation of microcracks in the inclusion/matrix interface in the as received material. The mixed inclusions predominated at the surface of the stainless steel studied.

In the cold deformed stainless steel (30%, 50% and 70%), the types of inclusions shown in Figure 2 were also seen at the surface, but in the material with 50% and 70% of deformation, the silicate type of inclusions predominated at the surface, comparatively to the alumina type. Besides, defects were created due to deformation process. Figures 3 to 6 show the effect of the levels of deformation on the types of inclusions found in the stainless steel investigated.

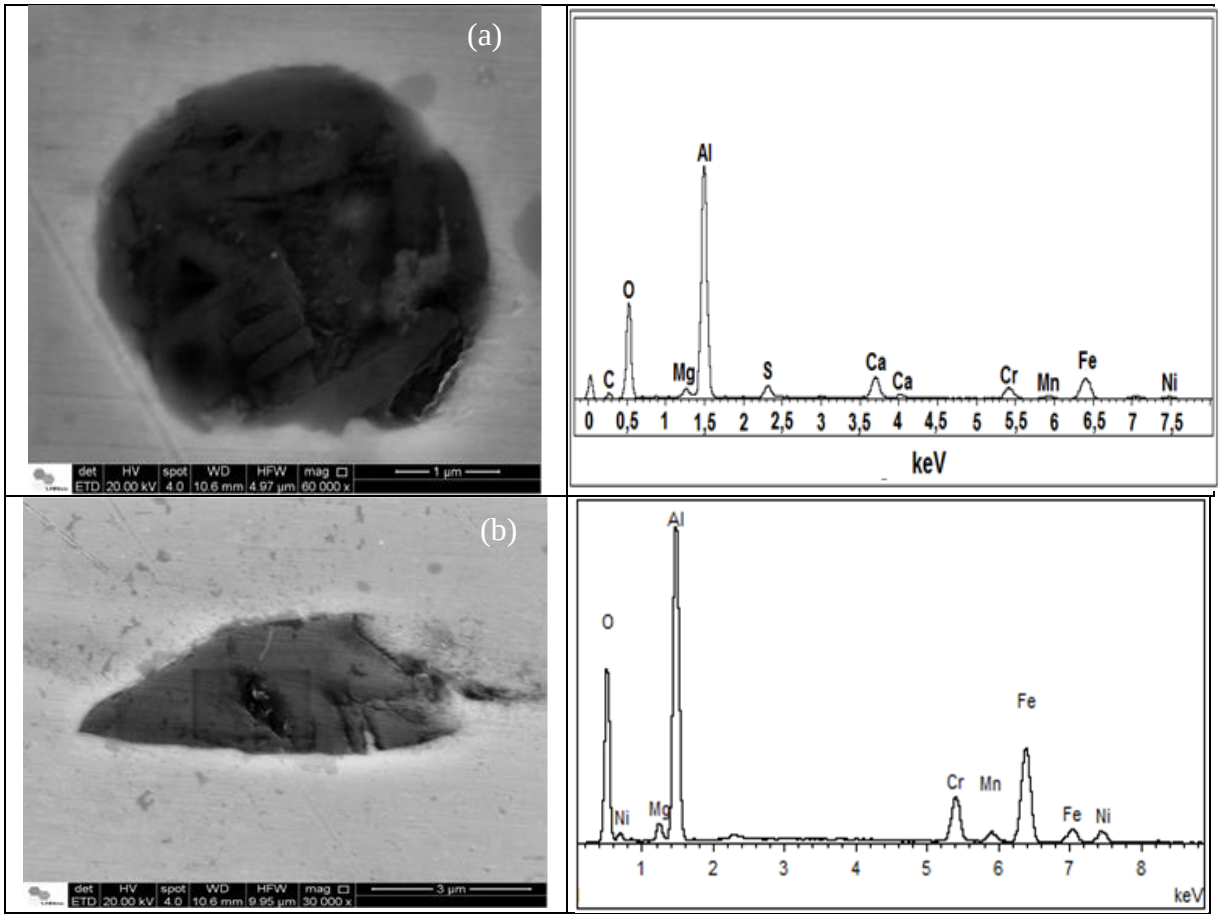

Figure 3. (a) Complex inclusions composed by a mixture of alumina, containing suphur and calcium abd (b) pure alumina inclusion found at the surface of the NBR 5832-1 stainless steel with 30% of deformation.

Figure 3 (a) shows a non-metallic and mixed inclusion which has been fragmented during the deformation process. EDX analysis carried out on this inclusion showed that it is a mixed inclusion mainly composed of aluminium oxide but also contains calcium, either as calcium oxide or calcium carbonate, and sulphur. Both, calcium oxide or calcium carbonate, are softer than the alumina and

could be more easily removed during cold deformation. This is clearly indicated in Figure 3 (a). The fact that this type of inclusion is mainly composed of alumina, although it contains calcium and sulphur, means that is brittle. Consequently brittle cracks (micro-cracks inside the inclusion) tend to be formed. Indeed, when this kind of inclusion is cold deformed, it becomes fragmented. Although the metallic matrix underneath the inclusion has not been exposed during the cold deformation, the softer material of the inclusion at the interface with the matrix has been removed, either during deformation or surface preparation.

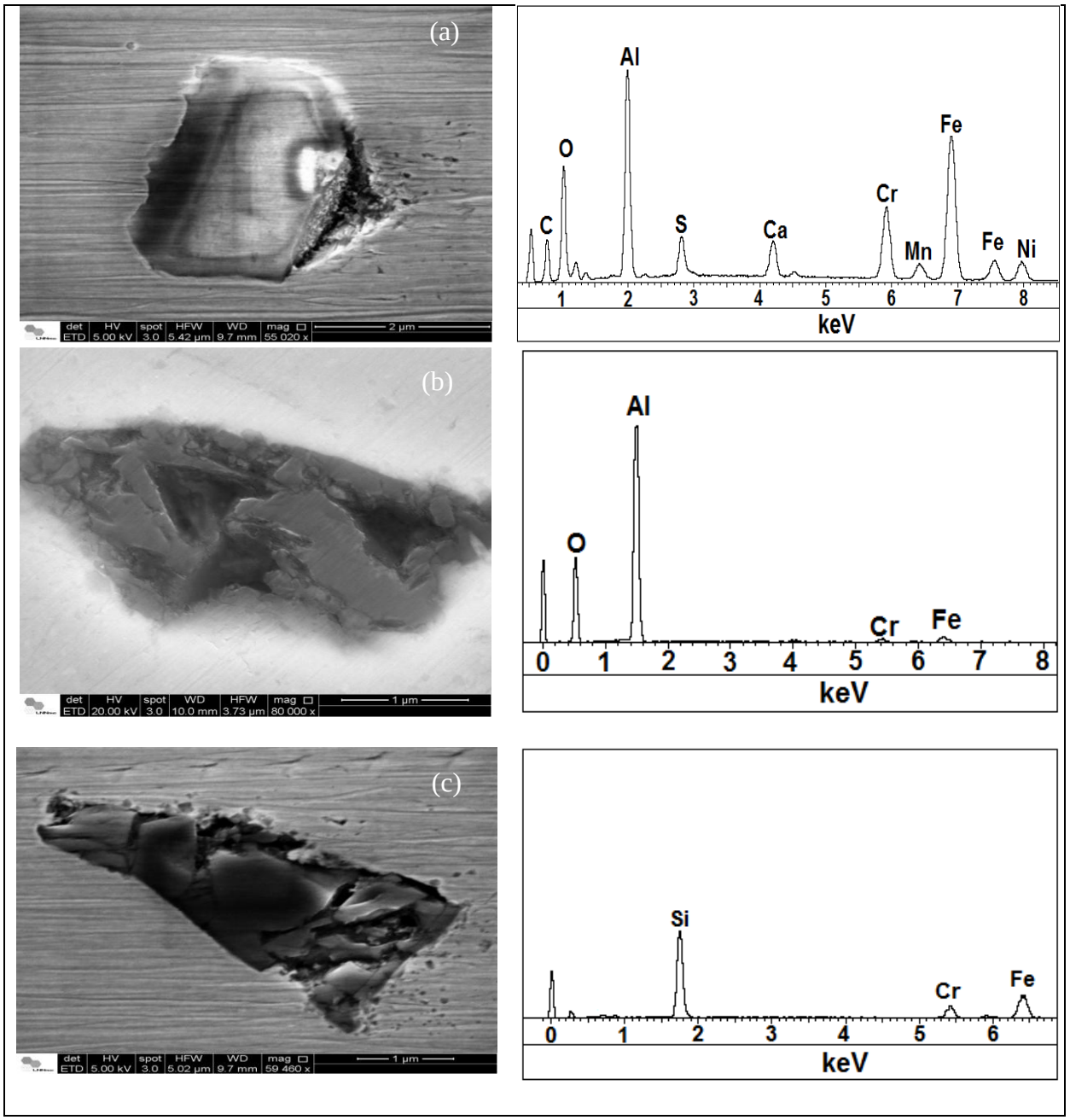

Figure 4. (a) Complex inclusion composed by alumina, calcium oxide, and sulphide; (b) alumina inclusion and (c) silica inclusion in the NBR 5832-1 stainless steel with 50% of deformation.

The removal of inclusion material at the interface with the matrix creates voids that might act as preferential sites for corrosive attack, eventually generating conditions that lead to crevices or pits. Figure 3(b) also supports the same observation found for the mixed inclusion shown in Figure 3 (a). The inclusion shown in Figure 3 (b) has also been fragmented during the deformation corresponding to 30% reduction in thickness. EDX analysis on this inclusion indicated a pure alumina inclusion which is of a brittle type.

The effect of cold deformation corresponding to 50% reduction in thickness on the microstructure of the stainless steel is shown in Figure 4.

Figure 4 (a) shows a non-metallic inclusion with fragmentation at one of the corners. EDX analysis performed on the inclusion shown in Figure 4 (a) showed it is a complex inclusion containing sulphur, aluminium and calcium, likely alumina-sulphide with calcium oxide. It is clearly seen that the cracked part of the inclusion material has been removed from the inclusion site leaving a void at the inclusion/matrix interface that is a shallow micro-crevice created during the cold deformation process. This is due to differences in the plasticity of the inclusion and the matrix. It is worth noting that for the mixed inclusion shown in Figure 4 (a), part of the matrix material was displaced and dispersed on top of the mixed inclusion alumina-sulphide. However, part of the same inclusion was also removed at its interface with the matrix creating defects that could act as crevices and favour localized corrosion during exposure to corrosive electrolytes.

When the material is deformed, the matrix will have higher deformation levels than the inclusion and, consequently, greater stresses are created at the matrix/inclusion interface producing voids in this region. During the deformation process, dislocations are displaced, and for materials with low stacking fault energy, dislocations displacement is difficult. Consequently, accumulation of dislocations occurs at non-metallic inclusions, generating high local stresses at this region.

Another important aspect to highlight is the fact that inclusions have lower plasticity when compared with the matrix and, consequently, higher stresses are generated at the matrix/inclusion interface. Moreover, in order to create a micro-crevice at the inclusion/matrix interface, some special conditions are required. The first is connected to the crystallographic orientation of the grains in contact with the inclusions, once grains with proper crystallographic orientation with respect to the applied force are more easily deformed. The second important factor is the number of bonds between the atoms of the inclusion and the matrix atoms. When the number of bonds is high, a great force is also required to break them. Indeed, if the stresses created are sufficiently high to break the bonds between the inclusion atoms and that of the matrix, micro-crevices are formed.

Figure 4 (b) shows a non-metallic inclusion which was fragmented during the deformation process. EDX analysis carried out on this inclusion showed that it is composed of aluminium oxide. This kind of inclusion suffered a brittle crack (micro-cracks inside the inclusion). Indeed, when this kind of inclusion is cold deformed, it tends to be fragmented. This type of defect is not harmful to pitting corrosion resistance, once the matrix underneath the inclusion has not been exposed. However, the exposure of the metallic material at the hedge with the intermetallics is possible and might favour localized attack.

Figure 4 (c) shows a silicate inclusion severally fragmented during cold rolling process. This is a ceramic type of inclusion that presents a brittle behavior. Indeed, when the material is deformed, the

brittle inclusions are fragmented creating micro-crevices, either within the inclusion or at the matrix/inclusion interface, as illustrated in this micrograph.

Silicon containing inclusions were not found at the surface of the SS with 30% of reduction in thicknes but a few of these were identified at the surface of the SS with 50% whereas they predominated in the samples with 70% reduction. In the material with 70% deformation, the silicate inclusions were severally fragmented with the formation of a highly cracked structure, during the cold rolling process, as Figure 5 shows. This type of ceramic inclusion has a brittle behavior. Indeed, when the material is deformed, the brittle inclusions are fragmented creating micro-crevices either within the inclusion or at the matrix/inclusion interface, as shown in Figure 5. In fact, the interface between this type of inclusion and the matrix showed voids that could promote localized corrosion such as crevice corrosion. However, the matrix material was also very much deformed by this level of cold deformation leading to shielding of the cracks and the voids created at the matrix-inclusions interface.

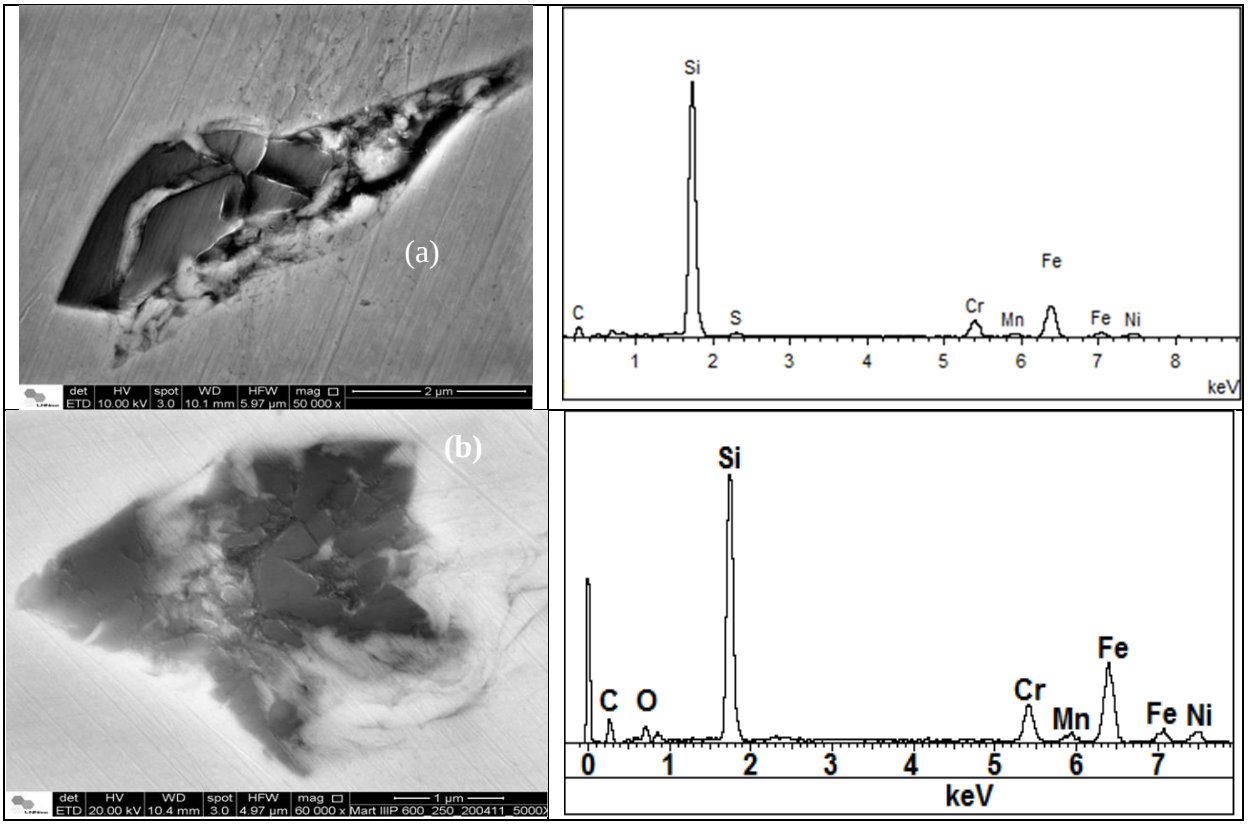

Figure 5. Micrographs of the NBR 5832-1 SS surface with cold deformation corresponding to 70% of thickness reduction. (a) Fragmented inclusion with the matrix material filling the voids between the cracks. (b) Matrix material covering the voids at the matrix-inclusion interface.

The effect of inclusions the localized corrosion resistance of stainless steels has been largely investigated in the literature [12-18]. The role of manganese sulphide inclusions on the pitting corrosion resistance has been particularly studied due to their frequent occurrence in commercial steels [12-15]. Manganese sulphide is harmful to the localized corrosion resistance due to its high solubility in chloridric acid environments. The dissolution of this type of inclusion creates preferential sites of pit

nucleation [16]. Lately, new development in the desulphurizing technology for stainless steel fabrication allowed the production of low sulphur stainless steels. Consequently, other types of inclusions, such as the oxide ones, became increasingly more important in the pitting corrosion of stainless steels [17,18]. At the same time, new researches [16,19] showed that oxide inclusions act as pit nucleation sites and allow their continuous growth.

It is important to note that the stainless steel used in the present study has a low sulphur content and, consequently, the amount of manganes sulphide inclusions is also low. Consequently, another type of inclusion, the mixed ones composed mainly of alumina, calcium oxide and silica, grow in importance for the corrosion resistance of the material tested without deformation.

Although the pitting resistance of stainless steels without cold deformation has been widely studied, there are few reported researches [18,20], on the effect of inclusions on the corrosion resistance of highly deformed material and this was the purpose of this investigation.

Deformation leads to stresses that are concentrated at the matrix and at the inclusions, leading to three types of microcracks, such as: microvoids or ductile cracks at the matrix/inclusion interface due to differences in the plasticity properties between the matrix and the inclusion; fragile cracks inside the inclusions and, cracks in the matrix (SS) at the neighbourhood of inclusions. The effect of cold deformation on the inclusions and the interface matrix-inclusions found in this work is supported by literature [21]. Microvoids might be formed at all temperatures at sites near to oxide the inclusions such as (Al_2O_3, $MnO.Al_2O_3$), which are hard. The silicates such as $MnO.SiO_2$ and $FeO.SiO_2$, on the other hand, do not present a ductile behavior at the temperature range from 25 ^oC to 900 ^oC, and, consequently, are associated to fragile cracks (inside the inclusions).

At high temperatures, the silicates are ductile and fragile cracks are rarely found. Besides, sulphide inclusions such as FeS, (Fe, Mn)S are ductile at all temperatures and cracks were found in the temperature range from 25 ^oC to 600 ^oC. However, voids are formed in consequence of plasticity differences between inclusions and the matrix. These voids are due to the difference in the mechanical properties of the two phases, matrix and inclusion. Voids of this kind have been reported in the literature at different temperatures [22].

The electrochemical behavior of the ISO NBR 5832-1 austenitic stainless steel, either without or with cold deformation, was characterized by electrochemical impedance spectroscopy (EIS) and the results are presented in Figure 6 as Nyquist and Bode phase angle diagrams. The Nyquist diagrams show a capacitive behavior associated to all tested materials, due to the passive film on their surfaces but the highest impedances were associated to the stainless steel with the highest degree of deformation (70%). The SS with 30% deformation showed impedances similar to that of the steel without deformation, although slightly lower, suggesting a deleterious effect of deformation on the passive film properties related to this degree of deformation.

The Bode phase angle diagrams shows a large plateau with phase angles varying from -65^o to -80^o from frequencies around 10^2 Hz to 10^{-2} Hz, that is, a fairly capacitive behavior typical of passive materials. These results also suggest the interaction of two time constants. For the stainless steel with 30% and 50% deformation, the phase angle decreases from the frequency corresponding to 1 Hz downwards. This is particularly evident for the steel with 50% deformation. The time constant at frequencies around 10^2 Hz is associated to the charge transfer that takes place at the passive

film/electrolyte interface, and the other at frequencies below 1 Hz related to the charge transfer at the substrate/passive film interface. It is important to highlight that the charge transfer starts at the passive film/electrolyte interface when the material is in contact with electrolyte, and the dissolution of metallic cations occurs at the metal/electrolyte interface. Consequently, the charge transfer also starts at the other interface in order to maintain the neutrality in the passive film. The phase angle diminution seen at frequencies below 1 Hz for the steel with 50% deformation is indicative that the charge transfer process at the substrate/passive film interface is being promoted by the charge transfer at the passive film/electrolyte.

Despite of the differences suggested by the EIS results, this technique provides a mean evaluation of the whole surface investigated which is covered by a passive film. However, the resistance of the passive film to breakdown is not indicated by this technique. Consequently, EIS by itself cannot provide a clear explanation for the differences found in the electrochemical behavior of the various conditions evaluated, mainly the resistance of the passive film to breakdown. The influence of the deformation on the pitting corrosion resistance of the material was investigated by potentiodynamic polarization tests and the results are shown in Figure 7.

The polarization curves show that the material with the highest degree of deformation (70%) presented the highest resistance to passive film breakdown. This result was supported also by the EIS one. This could be explained by the obstruction of the defects generated due to fragmentation of the inclusions by the matrix material which has been displaced into the defects, filling the voids during cold deformation, as Figure 5 shows. This phenomenon leads to a surface of higher corrosion resistance by protecting/covering the sites where aggressive species could accumulate and lead to localized corrosion with the passive film breakdown. On the other hand, the surface with the lowest resistance to film breakdown was the surface with 50% of deformation. This result is also supported by the EIS data and it is easily explained by the effect of deformation on the silicon containing inclusions causing their fragmentation and formation of voids/crevices at the interface between the matrix and the inclusions.

A comparison of the polarization curves of the material without deformation with that corresponding to 30% deformation shows slightly higher susceptibility to film breakdown associated to this last type material. Taking into consideration that the deformation corresponding to 30% of reduction in thickness did not expose the metallic substrate to the corrosive environment, the slight decrease in corrosion resistance of the deformed material might be related to the detrimental effects of deformation on the passive film properties.

It is worth pointing out that at the surface of the stainless without deformation or with 30% deformation, the same type of inclusions predominated. These were the complex inclusions of alumina mixed with calcium and sulphur. However, for the other levels of deformation (50% and 70%), the silicon oxide (silica or silicate) type of inclusion is the predominant type found at the surface.

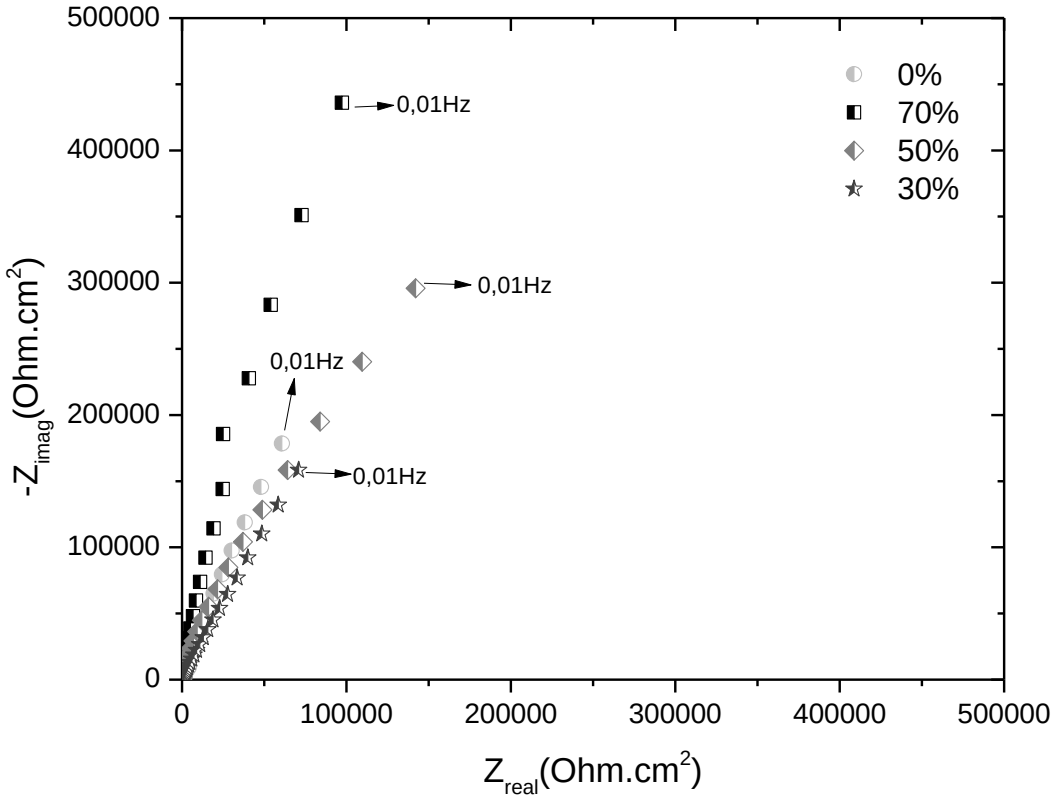

(a)

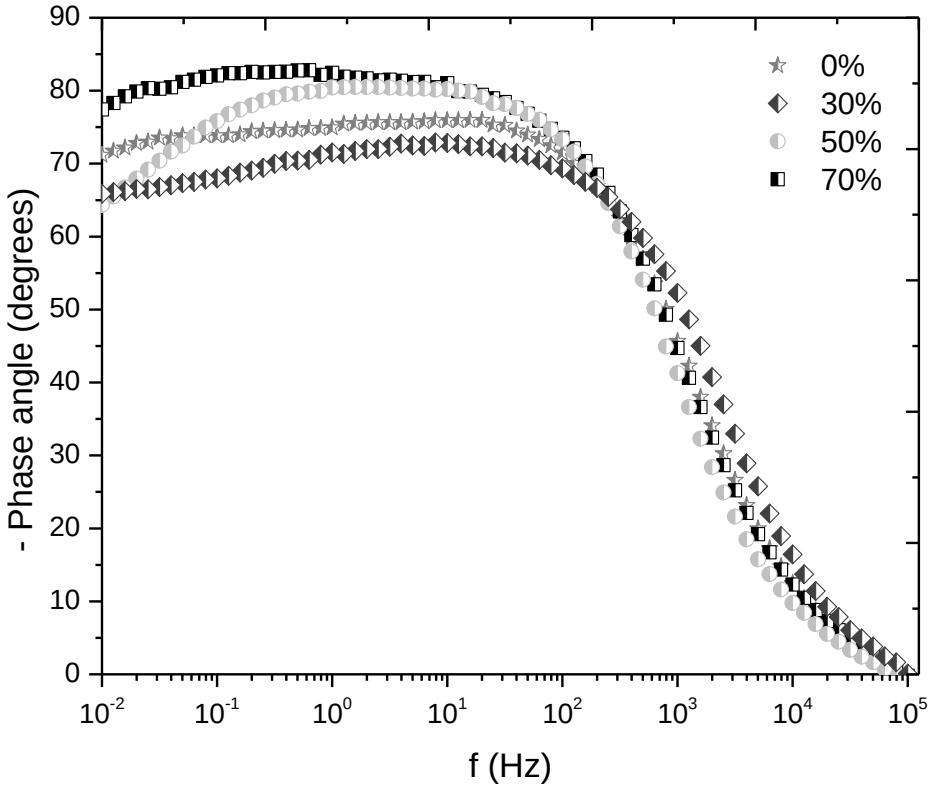

(b)

Figure 6. (a) Nyquist and (b) Bode phase angle diagrams of the ISO NBR 5832-1 austenitic stainless steel without and with deformation in a phosphate buffer solution.

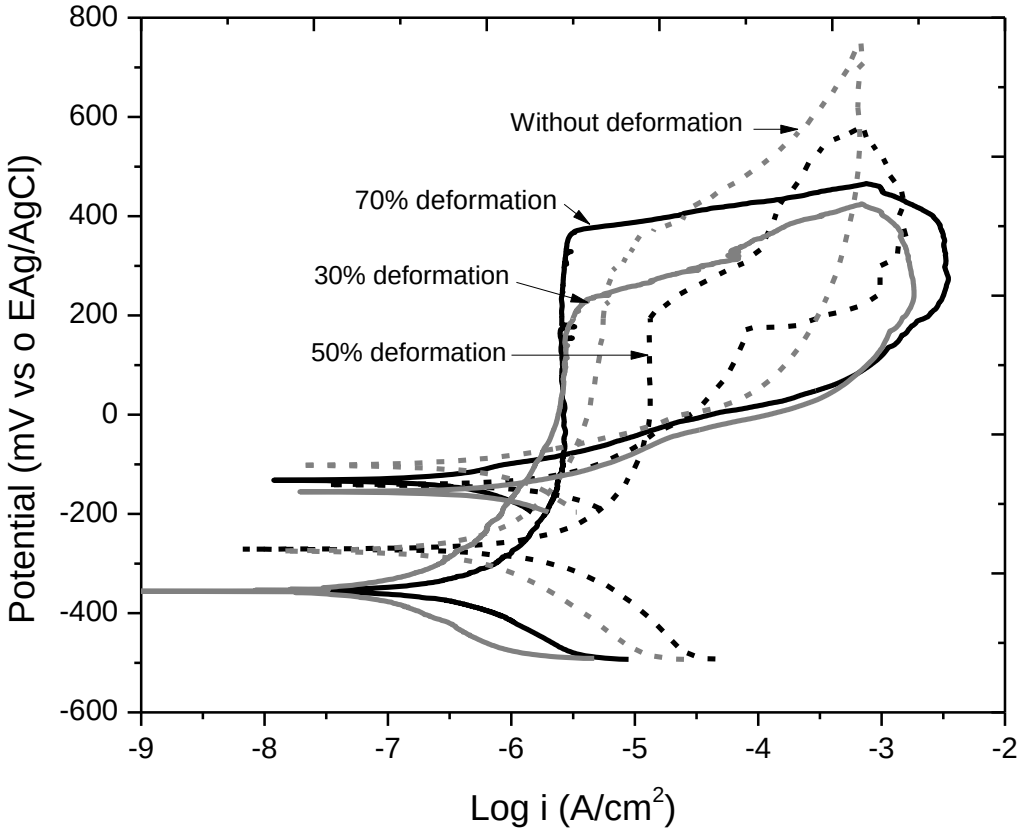

Figure 7. Cyclic potentiodynamic polarization curves of the ISO NBR 5832-1 austenitic SS without deformation and with various degrees of cold deformation.

In order to establish the influence of non-metallic inclusions on the pitting corrosion resistance and the correlation between the passive film breakdown and the microstructure at the surface, potentiodynamic polarization tests were performed in a sample of stainless steel with 50% deformation and interrupted at low current densities, soon after the pitting potential has been reached. The polarized surface was then investigated by SEM. Figure 8 shows that pit nucleation occurred in a non-metallic inclusion, which contains oxygen, aluminum, sulphur, magnesium and calcium. It is well known that calcium is added during the steel fabrication to desulphurize steel. Calcium modifies the morphology of the inclusions, making them round. After the polarization, it was found that the inclusion was dissolved at preferential sites (Figure 8), forming micro-crevices at the inclusion/matrix interface.

It is well known that the interfaces between the stainless steel matrix and the inclusions are the weakest sites in the passive film, being the most likely to break. Besides, as this kind of inclusion contains calcium in its chemical composition and the stainless steel has been exposed to the electrolyte which contains phosphate, it is possible that the calcium from the inclusion reacts with the phosphate from the electrolyte and, consequently, hydroxyapatite could form. Inside the micro-crevices, aggressive conditions are generated which promote autocatalytic corrosion conditions that hinder repassivation.

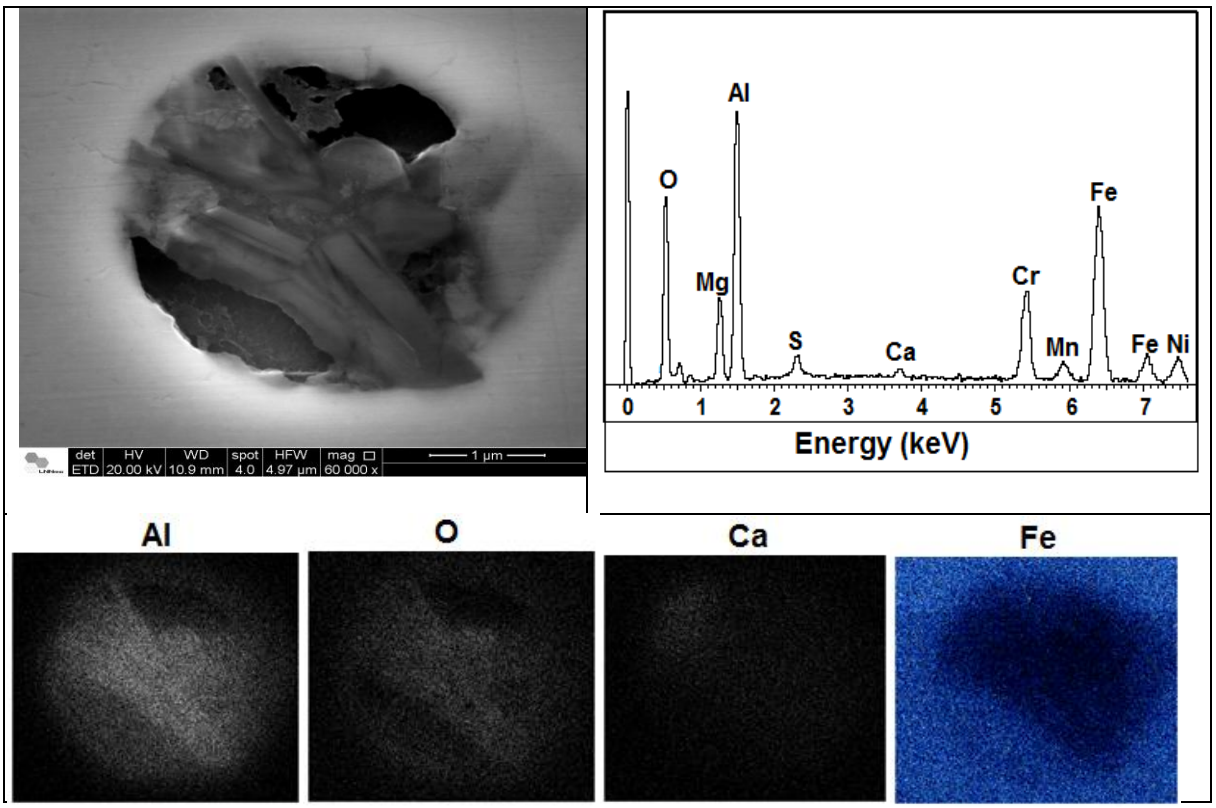

Figure 8. Differential dissolution of a mixed inclusion forming a micro-crevice at the inclusion/matrix interface.

Kamachi Mudali *et al.* [18] investigated the effect of cold deformation on the pitting corrosion resistance of three austenitic stainless steels, specifically 316L, 316LN and 316LHN. The grades of deformation used with these steels were 5%, 10%, 20%, 30% and 40%. The results showed that the pitting potential increased with deformation up to 20%; however, for higher deformation intensities, the pitting potential decreased. The authors suggested that for the steels with degrees of deformation until 20% there was a beneficial effect of surface diffusion on the formation of a more stable film ant this predominated over the deleterious effect of the deformation bands generated. On the other hand, the decreased pitting resistance for deformation grades above 20% was associated to the effects if deformation on the microstructure.

The influence of cold deformation on the pitting corrosion resistance of a high nitrogen stainless steel has also been studied by Yao Fu *et al.* [20]. They found that the pitting potential decreased with the degree of deformation and this was attributed to the microstructural modifications caused by deformation that are deleterious to the corrosion resistance. The deformation bands with their high density of dislocations are highly stressed areas that act as preferential sites for pitting [18]. Ravi Kumar *et al.* [23] also investigated the effect of cold deformation on the pitting corrosion resistance of the AISI 304L (S30403). They found that the volumetric fraction of martensite in the material increased with the degree of deformation. Besides, residual stresses increased with deformation degree up to 50%. However, for higher deformation levels, the residual stresses decreased in the austenite phase, but increase in the martensite one. Similarly to the results of the present study,

they also found that the pitting potential decreased with deformation up to a degree of 50%, but increased above this level.

The deleterious effect of cold deformation up to a degree of 50 % on the pitting resistance of the NBR ISO 5832-1 found in the present investigation might be related to high residual stresses induced by deformation. The prejudicial effects of high residual stresses on the material corrosion resistance have been reported in literature [24]. Even though, for the stainless steel with higher levels of deformation (70%), the increase in pitting potential, relatively to the material with lower levels of deformation, was associated to the blocking of voids and cracks, the effect of texture induced by deformation could also have improved the corrosion resistance of the tested material. The effect of texture on chromium diffusion favoring the formation of a protective chromium rich oxide film on the surface stainless steel has been largely described in literature [25-27].

4. CONCLUSIONS

The effect of cold deformation on the microstructure and localized corrosion resistance of the ISO NBR 5832-1 stainless steel has been investigated. The results showed a detrimental effect of deformation on the pitting resistance of the stainless steel for deformations corresponding to thickness reductions of 30% and 50%, whereas the localized corrosion resistance of the steel with 70% deformation increased comparatively to that without deformation. The decrease in pitting resistance was correlated with the defects created in the passive film, in the non-metallic inclusions (fragmentation) and at the interface between the non-metallic inclusions and the matrix during the cold deformation process leading to micro-crevices which are preferential sites for pitting nucleation. The very high levels of deformation (70% reduction in thickness) on the other hand, resulted in blocking of the voids and cracks with the matrix material, mainly at the interface between inclusions and the matrix.

ACKNOWLEDGEMENTS
The authors are grateful to FAPESP (Proc. 2012/50187-7) for the financial support provided to this work.

References

1. H. S. Khatak; B. Raj, *Corrosion of Austenitic Stainless Steel: Mechanism, Mitigation and Monitoring*. Alpha Science International Ltd., (2002)
2. Ihsan-ul-Haq Toor. *J. Electrochem. Soc.*, 158, No. 11(2011) C391.
3. N. E. Hakikia; M. Da Cunha Belo; A. M. P. Simões; M. G. S. Ferreira. *J. Electrochem. Soc.*, 145, No. 11, (1998) 3821.
4. A. Fattah-alhosseini; F. Soltani; F. Shirsalimi; B. Ezadi; N. Attarzadeh. *Corros. Sci.* 53 (2011) 3186.
5. M.Opiela; A. Grajcar; W. Krukiewicz, *Journal of Achievements in Materials and Manufacturing Engineering*, 33, n. 2, (2009) 159.

6. B. Surowska; A. Weronski, *Proceedings of the 14th International Scientific Conference "Advanced Materials and Technologies***"**, Gliwice Zakopane, p. 425-428,1995.
7. S. Zor; M. Soncu; L. Capan, *Journal of Alloys and Compounds*, 480 (2009) 885.
8. L. Peguet, B. Malki, B. Baroux, *Corrosion Science*, 49 (2007) 1933.
9. B.R. Kumar; B. Mahato; R. Singh, *Metallurgical and Materials Transactions, A 38* (2007) 2085.
10. H. Li; Z. Jiang; Q. Ma; Z. Li. *Advanced Materials Research*, 217-218 (2011) 1180.
11. M. Rutkowska-Gorczyca; M. Podrez-Radziszewska. *SIM XXXVI* (2009) 319.
12. P. Schmuki, H. Hildebrand, A. Friedrich, S. Virtanen, *Corrosion Science*, 47 (2005), 1239.
13. 13.G.S. Eklund, *Journal Electrochemical Society*, *121* (1974), 467.
14. D.E. Williams, R.K. Matt, C. John, G.I.N. Waterhouse, *Corrosion Science*, 52 (2010), 3702.
15. J. Stewart, D.E. Williams, *Corrosion Science*, 33 (1992), 457.
16. M.A. Baker, J.E. Castle, *Corrosion Science*, 33 (1992), 1295.
17. H.Y. Ha, C.J. Park, H.S. Kwon, *Corrosion Science*, 49 (2007), 1266.
18. U. Kamachi Mudali, P. Shankar, S. Ningshen, R.K. Dayal, H.S. Khatak, Baldev Raj, *Corrosion Science* 44 (2002) 2183.
19. A.H. Ramirez, A.M. Nocetti, N. Alonso Falleiros, *in: 66th Annual International Congress of ABM. São Paulo, SP, 2011, pp. 283-291.*
20. Yao Fu, Xinqiang Wu, Enhou Han, Wei Ke, Ke Yang, Zhouhua Jiang.: *Journal of The Electrochemical Society*, 155 (8) C455-C463 (2008).
21. F. Montheillet; P. Gilormini. *Journal of the Mechanics and Physics of Solids***,** 34, n. 2 (1986) 97.
22. T. Wegrzyn, M. Miros, *Transport Problems,* T. 2, n. 4 (2007) 87.
23. B. Ravi Kumar, Raghuvir Singh, Bhupeshwar Mahato, P.K. De, N.R. Bandyopadhyay, D.K. Bhattacharya, *Materials Characterization,* 54 (2005) 141.
24. H. E. Hanninen, *Int Metals Rev*, 3 (1979) 85.
25. C.L. McBee, J. Krugher, *Electrochimica Acta*, 17 (1972)1337.
26. A. Barbucci, G. Cerisola, P.L.Carbot, *Journal of Electrochemical Society,* 149 (2002) B534.
27. R.Singh, B. Ravi Kumar, A. Kumar, P.K. Dey, I. Chattoraf, *Metall Transactions;*34A (2003) 2148.